Article

Accurate Line Shapes from Sub-1 cm⁻¹ Resolution Sum Frequency Generation Vibrational Spectroscopy of α-Pinene at Room Temperature

Amanda L. Mifflin,[†,⊥] Luis Velarde,[‡,⊥,∇] Junming Ho,[§] Brian T. Psciuk,[§] Christian F. A. Negre,[§] Carlena J. Ebben,[∥,#] Mary Alice Upshur,[∥] Zhou Lu,[‡,¶] Benjamin L. Strick,[∥] Regan J. Thomson,[∥] Victor S. Batista,[§] Hong-Fei Wang,*[‡] and Franz M. Geiger*[∥]

[†]Department of Chemistry, University of Puget Sound, Tacoma, Washington 98416, United States

[‡]William R. Wiley Environmental Molecular Sciences Laboratory, Pacific Northwest National Laboratory, Richland, Washington 99352, United States

[§]Department of Chemistry, Yale University, P.O. Box 208107, New Haven, Connecticut 06520-8107, United States

[∥]Department of Chemistry, Northwestern University, Evanston, Illinois 60208, United States

Ⓢ *Supporting Information*

ABSTRACT: Despite the importance of terpenes in biology, the environment, and catalysis, their vibrational spectra remain unassigned. Here, we present subwavenumber high-resolution broad-band sum frequency generation (HR-BB-SFG) spectra of the common terpene (+)-α-pinene that reveal 10 peaks in the C−H stretching region at room temperature. The high spectral resolution resulted in spectra with more and better resolved spectral features than those of the Fourier transform infrared, femtosecond stimulated Raman spectra in the bulk condensed phase and those of the conventional BB-SFG and scanning SFG spectroscopy of the same molecule on a surface. Experiment and simulation show the spectral line shapes with HR-BB-SFG to be accurate. Homogeneous vibrational decoherence lifetimes of up to 1.7 ps are assigned to specific oscillators and compare favorably to lifetimes computed from density functional tight binding molecular dynamics calculations. Phase-resolved spectra provided their orientational information. We propose the new spectroscopy as an attractive alternative to time domain vibrational spectroscopy or heterodyne detection schemes for studying vibrational energy relaxation and vibrational coherences in molecules at molecular surfaces or interfaces.
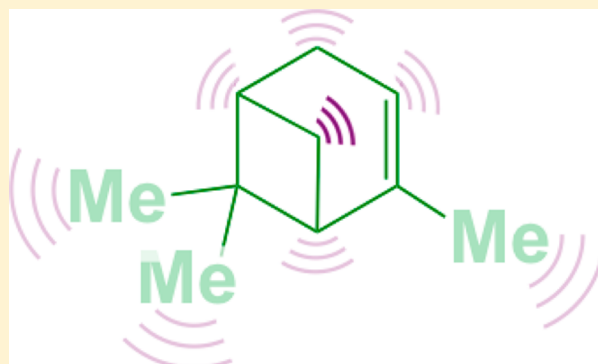
1. INTRODUCTION

Given the importance of terpenes in biology,[1] the environment,[2] and catalysis,[3] we find it curious that their vibrational spectra remain poorly understood. Wilson's classic paper of the vibrational spectroscopy of α-pinene,[4] one of the most abundant terpenes in nature,[1,5] reports only approximate assignments. Moscovitz and co-workers limited their analysis to experimental circular dichroism spectra of several monoterpenes without providing spectral assignments beyond circumstantial evidence.[6] Cheeseman and Frisch[7] recently reported normal mode frequencies obtained from high-level ab initio calculations of several terpenes but limited their analysis to frequencies below 1800 cm⁻¹, which is a congested spectral region.

Here, we present coherent C−H stretching spectra of α-pinene vapor in contact with CaF₂ windows that are collected with unprecedented 0.6 cm⁻¹ spectral resolution. We analyze their line shapes in order to determine the mode amplitudes,

frequencies, and phases with a level of accuracy that has, until now, been limited to a resolution of more than 5 cm⁻¹. This level of accuracy is an important achievement because it will serve as an experimental benchmark for computational studies on terpenes and provides vibrational decoherence lifetimes without the need for time domain vibrational spectroscopy. We demonstrate this ability by providing vibrational decoherence lifetimes computed from density functional tight binding (DFTB) molecular dynamics calculations that compare favorably to the values derived from the experiments. Moreover, our work represents an important step toward providing reliable, as opposed to hypothetical, vibrational mode assignments of this fascinating class of compounds.

Understanding the vibrational spectroscopy of terpenes is not nearly as straightforward as one might expect from a casual inspection of the molecule. This difficulty is in part due to the fact that terpenes contain several structural elements that one can expect to produce strong intramolecular vibrational coupling among the various oscillators across the entire mid-infrared region. For instance, significant strain in the four- and six-membered rings, as well as the C=C double bond, of α-pinene would perhaps lead one to think about strong vibrational coupling among its C−H oscillators, which can be probed by coherent spectroscopy, such as vibrational sum frequency generation (SFG) spectroscopy.[8−12]

SFG is an obvious choice to study the vibrational spectroscopy of constrained hydrocarbons because the SFG spectrum of a given surface-bound molecule is often better resolved than the corresponding condensed-phase infrared (IR) or Raman spectra at the same temperature or pressure conditions.[13−15] In addition, spectral interferences caused by the phase, or sign, properties of the oscillators provide additional spectral-resolving power in SFG that is absent in linear or other odd-order nonlinear spectroscopies.[10,16−18] Moreover, a set of polarization selection rules allows one to determine the symmetry of the vibrational transitions that give rise to particular spectral features.[13−15,19,20] Finally, the subwavenumber high-resolution broad-band SFG (HR-BB-SFG) spectrometer, recently developed at Pacific Northwest National Laboratory (PNNL), provides more than 1 order of magnitude improvement in spectral resolution when compared to conventional SFG spectrometers and has been shown to deliver nearly intrinsic SFG spectral line shapes for an accurate analysis of congested spectra.[15,18] These developments provide new opportunities for determining molecular structure by using surface and interfacial measurements as a means of expanding our molecular vibrational spectroscopy portfolio.

2. EXPERIMENTAL AND COMPUTATIONAL METHODS

A. High- and Standard-Resolution SFG Spectrometers. The details of the HR-BB-SFG spectrometer have been described in detail previously.[18] Briefly, we use two synchronized 1 kHz regeneratively amplified Ti:sapphire lasers. One is a nearly transform-limited ~90 ps laser (Legend Elite HE-ps, Coherent, Inc.), which is used to provide the upconverting visible pulse for the SFG measurement with subwavenumber resolution, and the other (Legend Elite DUO, Coherent, Inc.) is a sub-40 fs broad-bandwidth pulse, which is used to pump an optical parametric amplifier with difference frequency generation (OPA-DFG OPerA-Solo, Coherent, Inc.) to generate a mid-IR pulse with >400 cm^{-1} frequency coverage that spans the entire C−H stretching vibration frequency range of interest here (2800−3050 cm^{-1}) without additional tuning. At the sample, the incident angles of the visible and IR beams are 45 and 55° from the interface normal, respectively, and the energies of the visible and IR pulses are ~300 and ~28 μJ, respectively. The spectral resolution of 0.6 cm^{-1} of HR-BB-SFG was achieved with a 750 mm spectrograph (Andor Shamrock) equipped with a holographic 1800 lines/mm grating. The SFG signal was recorded by an electron-multiplied CCD camera (Andor Newton 971P) with 1600 × 400, 16 μm^2 pixels. Three 10 min sample and 10 min background scans were collected and normalized to z-cut quartz for each spectrum.

For comparison, we also used a standard-resolution broad-band (SR-BB) SFG spectrometer located at Northwestern University (NU), and a commercial picosecond scanning SFG spectrometer (EKSPLA) located at PNNL, both described in detail previously.[21,22] At NU, the visible probe pulse at 800 nm features a full width at half-maximum (fwhm) of about 1.5 ps, providing a spectral resolution of ~10−15 cm^{-1}, and the broad IR pulse is 150 fs long and covers about 150 cm^{-1} in each measurement, requiring use of Walker's hybrid scanning broad-band method,[23] as described earlier.[24] The incident angles and pulse energies for the NU system are 61° and ~1.5−2.5 μJ for the IR pulse and 42° and ~2 μJ for the upconverter pulse. The incident angles and pulse energies for the scanning system at PNNL are 56° and 180 μJ for the IR pulse and 45° and 200 μJ for the upconverter pulse, respectively. The 532 and 800 nm upconverters of the PNNL and the NU systems are off-resonance in the measurements. We probe the sample surface using the ssp polarization combination in order to sample those vibrational mode components that are oriented along the surface normal.[10] As all of the spectra were taken with the ssp polarization, the spectral line shape is independent of the laser incident angles,[10,17] and we find no effect on the spectra between the three spectrometers due to the incident angles and pulse energies, other than those that are due to their different resolutions.

B. Femtosecond Stimulated Raman Spectroscopy (FSRS). Similar to the setups of the broad-band femtosecond stimulated Raman gain and loss spectroscopy that were already described in the literature,[25,26] we substituted the 1−2 ps 800 nm laser pulse in the conventional FSRS with a synchronized ~90 ps laser pulse to achieve much higher spectral resolution as well as highly reproducible spectral line shapes, while a 40 fs laser is used to generate a white light continuum in a sapphire disk (450−960 nm) nm as the Raman pump beam for the stimulated Raman loss measurements.[15] The laser system for the FSRS measurement used the same two synchronized 1 kHz regeneratively amplified Ti:sapphire lasers as those in the HR-BB-SFG measurement described above. The stimulated Raman loss spectra were measured on the broad-band white light pump beam between 200 and 4500 cm^{-1} (while chopping the 800 nm probe at 20 Hz) using a 500 mm spectrograph (Andor Shamrock) equipped with a holographic 1200 lines/mm grating and a synchronized CCD camera (Andor Newton 940) with 2048 × 512, 13.5 μm^2 area pixels. With such detection, a resolution of ~1.4−1.6 cm^{-1} was achieved. A KG3 glass filter and a polarizer were used in the white light path, while the pulse energy for the 90 ps Raman probe ranged between 100 and 300 μJ.

To measure the FSRS spectra, less than 20 μL of liquid α-pinene was placed in a 2 mm × 2 mm × 50 mm fluorescence cell, where the pump and probe beams were set to cross at an angle of about 7°. Prior to detection, the broad-band pump beam intensity was adjusted by a neutral density filter, and the scattered light from the 800 nm probe beam was rejected by an appropriate notch filter. The spectra of the pump beam with the probe beam on and off were recorded and averaged for less than 1 min. The stimulated Raman spectra were obtained by taking the averaged ratio of the "probe on" and "probe off" spectral intensities.

C. Sample Cells. The SFG experiments were conducted by placing a few drops of α-pinene (Aldrich 268070, (+)-α-pinene, purity > 99%, and 305715, (−)-α-pinene, purity > 99%) into a shallow Teflon beaker that was subsequently covered with a 3 mm thickness and 25.4 mm diameter calcium fluoride window (WIN-3104, Red Optronics, Inc.). At PNNL, condensation of α-pinene on the CaF$_2$ window occurred within approximately

20 min when the window was completely sealed over the Teflon beaker, turning the window opaque. To alleviate this issue, the window was wiped clean with lens tissue between each 20 min sample and background collection period. Complementary experiments were carried out as well that avoided condensation of the α-pinene on the CaF_2 window by slightly displacing the window over the Teflon beaker so that vapor could escape from the beaker and equilibrate with the surface. Additional control experiments showed that leaving α-pinene samples outside of the refrigerator and in the laboratory air overnight introduced significant changes in the SFG spectra that are attributable to sample oxidation when exposed to air and room light. We therefore stored our sealed α-pinene samples in a refrigerator held at 4 °C in between experiments. All experiments were conducted at 22 ± 2 °C. At NU, a previously described Teflon cell[21] contained an exhaust hole through which any nonequilibrium state vapor was allowed to escape so that fogging of the optical windows did not occur.

D. Computational Methods. DFTB[27,28] molecular dynamics simulations in conjunction with displacement autocorrelation function[29−32] calculations were carried out to estimate the vibrational relaxation times of selected normal modes. The method involves construction of a distance matrix defined by the connectivity of the atoms in the molecule, that is, $[\vec{D}]_{ij}$ refers to the distance between atoms i and j. The time-dependent fluctuation of the distance matrix about its value at the equilibrium molecular geometry is shown in eq 2. Additionally, a static displacement matrix is defined where the molecular geometry is displaced by a specific step size along a particular normal mode (eq 3). Projection of the time-dependent fluctuation of the distance matrix on the displacement matrix in eq 4 is monitored as a function of time, and its Fourier transform yields a spectrum with a well-defined peak at the vibrational frequency of that normal mode. The peak is fitted to a Lorentzian, and the lifetime is estimated from the reciprocal of the fwhm.

$$[\vec{D}]_{ij} = |\vec{r}_i - \vec{r}_j| \tag{1}$$

$$[\vec{f}](t) = [\vec{D}](t) - [\vec{D}]_0 \tag{2}$$

$$[\vec{f}]_S = [\vec{D}]_S - [\vec{D}]_0 \tag{3}$$

$$P(t) = \sum_i^{N\,\text{atom}} \sum_j^{N\,\text{atom}} [\vec{f}]_{ij}(t)[\vec{f}]_{ij,S} \tag{4}$$

In the procedure described above, a selected normal mode is "excited" at the start of the simulation by displacing the molecule from its minimized geometry along that mode by a certain step size. The energy given to that normal mode therefore depends on the value of the step size. We have experimented with different step sizes ranging from 0.5 to 0.0625 Å and found that the calculated vibrational lifetimes are relatively insensitive to the choice of step size (see Table S1 in the Supporting Information). Using the βCH_2 symmetric stretch as an example, these displacements span an energy range of 2−150 kcal mol^{-1}, while the excitation energy of this mode (2929 cm^{-1} at the DFTB level) is approximately 8.5 kcal mol^{-1}. On this basis, we have adopted the smallest step size of 0.0625 Å because the normal mode representation is likely to be most valid when the displacement is small. The lifetimes are averaged over five 6 ps trajectories under the *NVT* ensemble at 300 K using the Berendsen thermostat with a coupling strength

of 0.1 ps^{-1}. The time step of 0.2 fs is used to propagate the classical trajectories. Full computational details, displacement decay plots, and corresponding Fourier transform are provided in the Supporting Information.

3. RESULTS AND DISCUSSION

A. Sub-1 cm^{-1} Resolution SFG Spectroscopy Resolves More Spectral Peaks than Conventional Broad-Band and Scanning SFG. We find no noticeable difference in the ssp-polarized SFG spectra of (+)-α-pinene and (−)-α-pinene vapor at the optical window surfaces used here. Moreover, complementary data shown in the Supporting Information (Figure S1) indicate that (−)-α-pinene synthesized at NU and commercially available (−)-α-pinene produce comparable high-resolution SFG spectra. The data discussed in this report are all taken with commercially available (+)-α-pinene, which we refer to as α-pinene in the remainder of this work.

In our previous report of the first vibrational SFG spectrum of α-pinene collected using conventional BB-SFG,[21] we referred to published SFG spectra of compounds containing linear hydrocarbon chains[24,33−49] to attribute the SFG signal at 2960 cm^{-1} to the asymmetric methyl C−H stretch, the intensity at 2940 cm^{-1} to a methyl Fermi resonance, and the one at 2880 cm^{-1} to the symmetric methyl C−H stretch. Guided by literature precedent,[33,50−53] we also stated that the methylene group on the four-membered ring of α-pinene may contribute SFG signal intensity between 2950 and 2990 cm^{-1} due to ring strain. Our current study identifies a number of additional peaks that will aid in producing reliable spectral mode assignments of α-pinene. Work toward reaching this goal, which pairs SFG spectroscopy of isotopologues of α-pinene with density functional theory and molecular dynamics calculations, is ongoing and beyond the scope of this paper. Instead, we focus here on a comparison to available literature data and the determination of accurate phases and lifetimes from the sub-1 cm^{-1} resolution SFG spectra.

Figure 1 shows the ssp-polarized SFG spectra of α-pinene collected with spectral resolutions of $\sim$6, $\sim$15, and $\sim$0.6 cm^{-1}. As expected, a number of features present in the 0.6 cm^{-1} resolution spectrum are obscured in the lower-resolution SFG spectra. Most notably, the 0.6 cm^{-1} resolution SFG spectrum clearly shows several distinctive peaks and shoulders in the
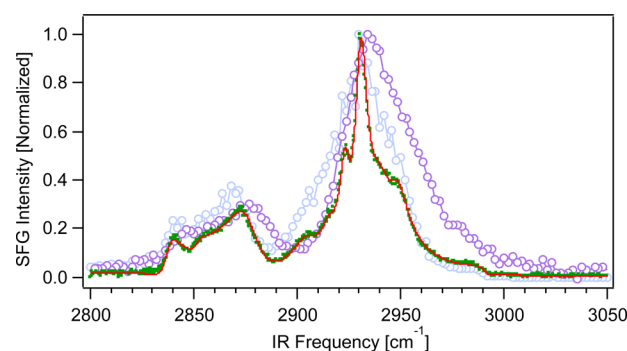
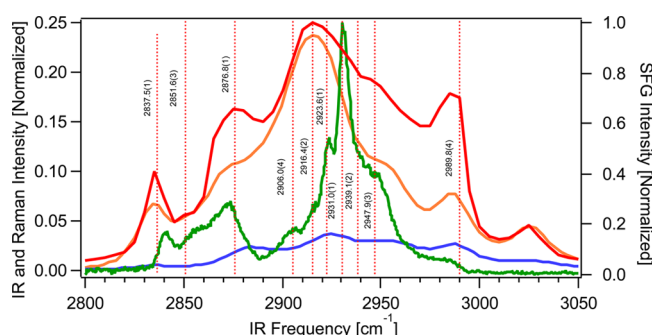

Figure 1. Comparison of the ssp-polarized SFG spectra of α-pinene vapor in contact with a CaF_2 window probed using a spectral resolution of 0.6 cm^{-1} (green dots, HR-BB-SFG at PNNL), 6 cm^{-1} (blue circles, scanning SFG, PNNL), and 15 cm^{-1} (purple circles, SR-BB-SFG, Northwestern University), and fit to 0.6 cm^{-1} spectrum (red line). The spectral intensities are normalized at the highest peak position.

2890–2960 cm^{-1} frequency region that are not resolved using the other instruments. The sharp peak at ~2930 cm^{-1}, in particular, clearly demonstrates the resolving power of the HR-BB-SFG spectrometer. The fwhm of this sharp peak is less than 10 cm^{-1} (about 7.6 cm^{-1} from the fitting results to be discussed below). It has been shown recently that for spectral features with a fwhm in the range of 5–10 cm^{-1}, the instrumental spectral resolution should be at least 2 cm^{-1} in order to obtain SFG spectra with good line shape.[54]

B. Sub-1 cm^{-1} SFG Spectroscopy Resolves More Peaks than Fourier Transform IR (FTIR) and FSRS. In SFG, the peak position and width and assignments of the surface molecule spectrum are usually compared with the IR and Raman spectra of the same molecule in the liquid phase or in liquid solution. This may work to a certain extent for simple chain molecules[10,13,14] but usually not as well for the molecules with rings or other complex structures.[15] To illustrate this, we compare literature FTIR data from the NIST database, FSRS spectra with the pump and probe electric field polarizations parallel and perpendicular to each other, and the HR-BB-SFG spectra of α-pinene in Figure 2, all with similar spectral

Figure 2. Comparison of the ssp-polarized HR-BB-SFG spectrum of α-pinene adsorbed on a CaF$_2$ surface (green) and the FTIR (red, 2 cm^{-1} resolution) and femtosecond stimulated raman spectra (FSRS, orange and blue for parallel and perpendicular polarization, respectively, 1.6 cm^{-1} resolution) of α-pinene liquid. The calibrations of the spectrometer in the HR-SFG and FSRS measurements are within 1 cm^{-1}. The FSRS spectral intensity is the percentage of the Raman intensity loss. The FTIR intensity was normalized to its highest peak intensity for comparison. The vertical dotted lines are the peak positions from the fitting procedure carried out on the HR-BB-SFG spectra.

resolution. The data show that the line shape, peak position, and width are quite different between the surface HR-BB-SFG spectrum and the IR or Raman spectra of the same molecule in liquid solution.

The FTIR (2 cm^{-1} resolution) and FSRS spectra (1.6 cm^{-1} resolution) display similar apparent peaks, with slight shifts in peak positions and some minor differences in the relative intensities. While the overall spectral line shapes are significantly different, the FTIR, FSRS, and HR-BB-SFG spectra share apparent peaks at approximately 2835–2845, 2850–2855, 2870–2875, 2910–2930, 2945–2955, and 2985–2990 cm^{-1}. Out of these peaks, the only one not reported by the seminal work of Wilson from 1976[4] is the one at 2850–2855 cm^{-1}. The sharp peak at around 2930 cm^{-1} is not present in either the FTIR or FSRS spectra; however, the broad peak centered at ~2925 cm^{-1} in the FTIR and FSRS spectra may[10] be a combination of the sharper 2930 and 2925 cm^{-1} peaks observed in the HR-BB-SFG spectrum. The peak at around

3030 cm^{-1} is present in both the FTIR and FSRS spectra and listed in Wilson's reported spectral data table,[4] but it is largely absent in the HR-BB-SFG spectrum unless one specifically centers incident IR energy right at that frequency, indicating that it is most likely associated with a C–H oscillator oriented predominantly perpendicular to the probe direction.

From the parallel and perpendicular FSRS spectra, it is not clear how to obtain accurate depolarization ratios of the many overlapping peaks in the Raman spectra, which are often helpful for orientation analyses.[55–57] However, the intensities of almost all of the spectral features are much stronger in the parallel spectra when compared to the perpendicular spectra reported here. Such small Raman depolarization ratios indicate that almost all of the apparent spectral features have the characteristics of symmetric CH$_2$ or CH$_3$ stretches in the α-pinene molecule.[58] This fact is consistent with the SFG polarization selection rules that the symmetric CH$_2$ or CH$_3$ stretching mode should be dominant in the ssp polarization.[10,13,19]

The striking differences between the line shapes of the 0.6 cm^{-1} resolution SFG spectrum and the FTIR and Raman spectra indicate differences in the intramolecular interactions of α-pinene at the CaF$_2$ surface as compared to its pure liquid condensed phase. As discussed above, the ~2930 cm^{-1} mode that is so prominent in the 0.6 cm^{-1} resolution is noticeably narrow, indicating a long decoherence lifetime. The significantly broadened FTIR and Raman spectra in this frequency range, which were collected in the condensed phase, suggest that there are significant intermolecular interactions in the α-pinene liquid that affect the decoherence of the vibrational motion of the oscillator that gives rise to signal at 2930 cm^{-1}. Such intermolecular interactions are unlikely to contribute to dephasing in the SFG spectra, which were collected at the vapor/solid interface. These observations indicate that a direct comparison between the surface and bulk vibrational spectra of the same molecule can reveal detailed information on molecular structure and interactions in different chemical environments, as well as energy flow within a given molecule as its oscillators may be subject to intramolecular energy redistribution (IVR).

C. Spectral Fitting Quantifies Peak Positions, Amplitudes, and Bandwidths of Ten Modes Accurately. As discussed in detail previously,[15] when fitting the HR-BB-SFG spectrum in the C–H stretching vibration region, inhomogeneous broadening effects are usually (even though not always) small and can be carefully neglected as significant inhomogeneous effects in the spectral line shapes would result in deviations of the fitting results from the spectral data. Thus, the following fit function is applicable

$$I_{SFG} = \left| A_{NR} + \sum_q \frac{A_q}{(\omega_q - \omega_{IR}) - i\Gamma_q} \right|^2 \tag{5}$$

In the expression, A_{NR} is the nonresonant term, and A_q, ω_q, and Γ_q are the amplitude, frequency, and width parameters, respectively, of the homogeneous line shape or the Lorentzian line shape of the qth mode. Here, the phase angle ψ_{NR}, as in eq 6, is dropped when the baseline is almost zero, suggesting insignificant nonresonant contributions and straightforward phase relationships. With SR-BB-SFG and scanning SFG, spectral fitting with many overlapping peaks may generate unstable or even unphysical fitting parameters if the line shape is not accurate (usually associated with SR-BB-SFG) or if the

number of experimental data points (i.e., pixels per cm^{-1}) is not enough (usually associated with scanning SFG) to allow the determination of an extensive number of parameters. In both cases, it is often difficult to know how many absorption lines are present in a congested spectrum, that is, fitting congested spectra is often not unique. HR-BB-SFG appears to be a viable solution to both problems.[15]

Here, fitting parameters with 10 peaks to the HR-BB-SFG spectrum is not only stable but also physically reasonable as the HR-BB-SFG spectra not only have accurate line shape but also ample data points to allow determination of the number of fitting parameters. It is obvious that it is impossible to fit the SR-BB-SFG or the scanning SFG spectra in Figure 1 with stable and physically meaningful fitting parameters for more than four Lorentzian peaks. The solid red line in Figure 1 shows a nearly perfect fit to the HR-BB-SFG spectra with 10 Lorentzian peaks. The fitting parameters are listed in Table 1. Also in Figure 2, the peak positions listed in Table 1 are labeled and represented by vertical dashed lines. One can see clearly that these resonances match the peak positions in the FTIR and FSRS Raman spectra nicely, except for (1) the 3030 cm^{-1} peak that is absent in the ssp SFG spectrum and (2) the peaks in the 2900−2950 cm^{-1} region, where the FTIR and Raman spectra are congested and not well resolved. Test fit results with less or more than 10 Lorentzian peaks turned out to be significantly less satisfactory. With eight or nine peaks, the fitting results apparently miss the spectral line shape at the shoulders of the 2900−2960 cm^{-1} region, and the fitting curves show significant residues from the HR-BB-SFG spectrum in this region in comparison to the fitting curve containing 10 peaks. Alternatively, adding more than 10 peaks to the fit function can generate fitting curves that are comparable to those obtained with 10 peaks; however, doing so also produces nonphysical bandwidths for the additional peaks that always closely overlap with each other. Therefore, we find the best fit to the HR-BB-SFG spectrum with 10 Lorentzian peaks. Similarly, a 12 Lorentzian peak fitting was successfully applied to the C−H stretching vibration region in the HR-BB-SFG spectrum of a cholesterol molecule at the air/water interface with the same spectral resolution and similar signal-to-noise. The parameters thus obtained were successfully used to generate the time-dependent SFG spectra of the cholesterol molecule with lower spectral resolution and thus confirmed the validity of the fitting and the accuracy of the fitting parameters.[15] Here, we show that the fitting parameters from the HR-BB-SFG spectrum of α-pinene can be successfully used to simulate the lower-resolution spectra as well.

D. Line Shapes Produced by Sub-1 cm^{-1} SFG Spectroscopy Are Accurate. Given the robustness of our fit parameters for the HR-BB-SFG spectra, especially the sign of the amplitude parameter A_q, we used them to quantitatively simulate and predict the SFG spectra with lower spectral resolution, similar to the reported simulation to the spectra of the cholesterol molecule with lower resolution and with different delay times between the IR and visible pulses.[15] To do so, we used the following convolution of a Lorentzian and a Gaussian line shape function, as often used to approximate the condensed-phase vibrational spectral line shape,[15] to simulate the SFG spectra with different spectral resolutions

Table 1. Fit Results

	χ_{NR}	peak 1	peak 2	peak 3	peak 4	peak 5	peak 6	peak 7	peak 8	peak 9	peak 10
ω_i (cm^{-1})		2837.4(1)	2851.4(3)	2876.7(1)	2905.9(4)	2916.4(2)	2923.5(1)	2930.9(1)	2939.1(2)	2948.0(3)	2989.9(4)
A_i	−0.045(3)	−1.10(4)	−0.20(4)	3.6(1)	1.5(2)	0.8(2)	0.95(8)	2.5(2)	3.8(7)	0.9(3)	−0.42(6)
Γ_i (cm^{-1})		4.1(2)	3.3(6)	9.7(2)	8.1(6)	5.1(7)	3.1(2)	3.8(1)	9.0(2)	5.1(6)	4.1(7)
τ (ps)^a		1.29(5)	1.6(3)	0.55(1)	0.66(5)	1.1(1)	1.72(8)	1.40(4)	0.59(7)	1.0(1)	1.3(2)

^{a}The vibrational decoherence lifetime is $\tau = 1/2\pi c\Gamma_i$, where c is the speed of light. Uncertainties to the point estimates are given in parentheses next to the corresponding significant figure.

$$I_{SFG} \propto |R^{(2)}(\omega_{IR})|^2$$

$$= \left| A_{NR} e^{i\psi_{NR}} + \sum_q \frac{A_q}{(\omega_q - \omega_{IR}) - i\Gamma_q} \otimes e^{-\omega_{IR}^2/2\Delta\omega_q^2} \right|^2$$

(6)

Here, $A_{NR} e^{i\psi_{NR}}$ is the nonresonant response, with the nonresonant amplitude A_{NR} and phase angle ψ_{NR}, and the rest of the expression is the vibrationally resonant response. The resonant response function is the sum over all of the line shape functions of the contributing vibrational modes (or states), which is the convolution function (represented by the operation $\otimes$) of the Lorentzian line shape and the Gaussian line shape function. In the expression, A_q, ω_q, and Γ_q are the amplitude, frequency, and width parameters, respectively, of the homogeneous line shape or the Lorentzian line shape of the qth mode, and $\Delta\omega_q$ is the width parameter of the inhomogeneous line shape function or the Gaussian line shape function of the qth modes. Note that the fwhm of a Lorentzian line shape is the so-called homogeneous width $\Delta\nu_H^q = 2\Gamma_q$, while the fwhm of a Gaussian line shape is called the inhomogeneous width $\Delta\nu_I^q = 2(2\ln 2)^{1/2}\Delta\omega_q$. The homogeneous decoherence lifetime is given by $\tau_q = 1/2\pi c\Gamma_q$, where c is the speed of light.[15]

When there is no significant contribution from the inhomogeneous broadening, $\Delta\omega_q = 0$, that is, the Gaussian function becomes a δ function, and eq 6 is reduced to eq 5 when the phase angle ψ_{NR} is dropped. However, when the spectral resolution is finite, the spectral resolution function is usually a Gaussian function because the laser profile of the visible pulse usually is or is usually close to a Gaussian function,[15] unless the laser profile is intentionally chirped or reshaped.[59−61] Therefore, one can use the spectral resolution width parameter to modify the $\Delta\nu_I^q$ parameter (all of the modes should have the same instrumentation broadening value) and then use eq 6 and the fitting parameters in Table 1 to simulate the spectrum with different spectral resolutions. It is known that when discussing the fwhm of the Gaussian function, the fwhm of the intensity Gaussian function is $1/\sqrt{2}$ of the electric field Gaussian function.[62] Furthermore, it is straightforward to show that the fwhm of the time domain Gaussian intensity profile and the fwhm of the corresponding transform-limited frequency domain Gaussian intensity profile have a simple relationship of $\Delta t \cdot \Delta\nu \approx 14.7$ when Δt is in units of picoseconds (10^{-12} second) and $\Delta\nu$ is in units of the commonly used wavenumber (cm^{-1}). Therefore, when the resolution is $\Delta\nu = 6$ cm^{-1}, the corresponding $\Delta t = 2.45 \approx 2.5$ ps, and when the resolution is $\Delta\nu = 10$ cm^{-1}, the corresponding $\Delta t = 1.47 \approx 1.5$ ps. Of course, in all experiments, the time domain and the frequency domain laser profiles are not necessarily ideal transform-limited Gaussian line shapes. Therefore, we can only find the equivalent Gaussian profile to make the simulations of the lower spectral resolution spectra. For the picosecond scanning SFG spectrum with 6 cm^{-1} resolution, we use the equivalent 2.5 ps fwhm of the transform-limited Gaussian time domain profile to make the simulation, and one can see below that this simulation gives quite satisfactory simulation of the spectrum in Figure 3b, while to simulate the SR-BB-SFG spectrum, we found that an equivalent 1.5 ps fwhm of the transform-limited Gaussian time domain profile gives the closest simulation of the spectra, as in Figure 3c.

Figure 3 compares simulated SFG spectra using the fitting parameters listed in Table 1 with different spectral resolutions.
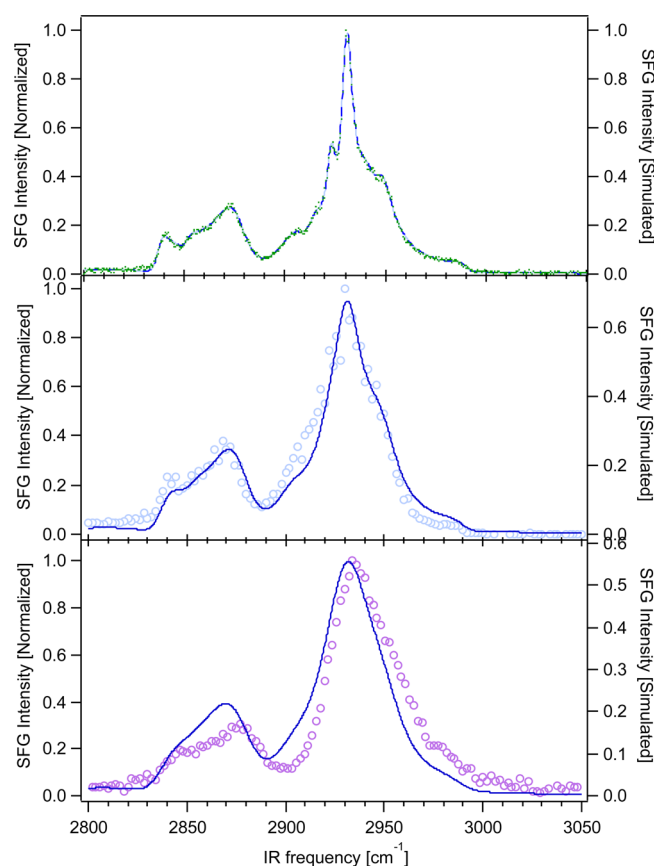
Figure 3. Comparison of the SFG spectra with the simulated SFG spectra from the Fourier transformation of the vibrational coherence calculation using the spectral amplitude, peak position, and width parameters from the Lorentzian line shape fitting of the HR-BB-SFG α-pinene spectrum, obtained using infinite (dashed) and 90 ps (solid blue line) Gaussian upconverter pulses (top) and upconverters having fwhm values of 2.5 (middle) and 1.5 ps (bottom), corresponding to 6 and 10 cm^{-1} spectral resolution, respectively.

The spectra simulated with 0 cm^{-1}, that is, hypothetically infinite, spectral resolution and the spectra simulated with 0.6 cm^{-1} spectral resolution match almost perfectly with each other, indicating that the 0.6 cm^{-1} spectral resolution measurement introduces no noticeable effect on the intrinsic spectral line shape. Further simulation suggests that if the spectral resolution is less than 2 cm^{-1}, most of the spectral features, except the sharp 2930 cm^{-1} peak, shall remain with unnoticeable deviation from the ideal spectrum with 0 cm^{-1} spectral resolution. Such simulation suggests the upper limit for the spectral resolution that will ensure measurement of the intrinsic spectral line shape with spectral features as narrow as a few wavenumbers.

As the spectral resolution gets worse, the height (spectral intensity) of the narrower peaks (with smaller Γ_q values) would be significantly reduced in comparison to that of the relatively broader peaks (with bigger Γ_q values). This is what was observed in the SFG spectra measured with lower spectral resolution. Figure 3b shows that the spectrum simulated with 6 cm^{-1} resolution agrees quite well with the experimental 6 cm^{-1} resolution spectrum measured with the scanning SFG spectrometer. It was shown previously that with eq 6 and the fitting parameters of 12 overlapping peaks from the HR-SFG-VS spectrum of a cholesterol monolayer, the lower-resolution SR-SFG-VS spectra of the same cholesterol surface, obtained
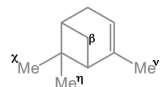
with known laser profile parameters with different time delays, can be quantitatively reproduced.[15] Therefore, the small deviation between the measured spectra from the simulated spectra in this study is most likely the result of the laser profile in the experiment that deviated from the ideal transform-limited Gaussian as used in the simulation. Nevertheless, the simulation can be considered quite satisfactory in comparison to the experimental data. Most importantly, one can see how many spectral details are lost at the spectral resolution of 6 cm^{-1} and why sub-1 cm^{-1} spectral resolution is essential in measurement and analysis of spectra with many overlapping narrow peaks. Without enough spectral resolution, one cannot take advantage of the coherent and interference nature of the spectral features in the SFG spectra.

Figure 3c shows that the spectrum simulated with the 1.5 ps fwhm transform-limited Gaussian laser profile, that is, with 10 cm^{-1} spectral resolution, agrees reasonably well with the experimental SR-BB-SFG spectrum. Even though the main spectral features of the simulated and measured spectra match each other, there are more significant deviations than those in the 6 cm^{-1} simulated and experimental spectra in Figure 3b. These deviations may come from different sources. First, the experimental visible laser pulse in the SR-BB-SFG may not follow an ideal transform-limited Gaussian function; second, when the visible pulse is only 1−2 ps, chirp in the visible and IR pulses may also introduce an additional degree of distortion of the measured SFG spectra from the intrinsic SFG responses of the molecular surface; third, the procedures to collect spectra with different IR pulses and then to patch them may also introduce uncertainties to the spectral line shape. Whichever is the cause of the difference, detailed discussion on each of them is beyond the scope of this study. Nevertheless, the comparison of the simulated and measured spectra with different spectral resolutions suggests that the reliable spectral line shape of the HR-BB-SFG spectrum not only allows us to obtain much more detailed spectral parameters from fitting the spectra, but also, the parameter thus obtained can be used to reproduce or predict the spectra measured under different conditions. Therefore, the spectral parameters are reliable and are the closest representation of the intrinsic spectral properties of the molecular surface, if not the exact.

E. Accurate Lineshapes Yield a Reliable Lifetime and Phase for Each Oscillator. As established herein, the HR-BB-SFG intensity spectrum yields accurate line shape parameters because the experimental resolution is so much smaller than the natural line widths of roughly 5−10 cm^{-1}.[15,54] It follows, then, that the corresponding homogeneous decoherence lifetimes obtained should be reliable. Table 1 lists the corresponding homogeneous decoherence lifetimes, which are found to span a factor of 3, ranging from 0.55 (2876.7 cm^{-1}) and 0.59 ps (2939.1 cm^{-1}) to 1.4 (2930.9 cm^{-1}) and 1.72 ps (2923.5 cm^{-1}). In comparison to the conventional or SR-BB-SFG, the ability of HR-BB-SFG to experimentally determine vibrational modes with significantly different decoherence lifetimes may shed light on the understanding of the detailed mechanisms of the intra- and intermolecular coupling and vibrational relaxation processes.

To further investigate the vibrational decoherence lifetimes, we employed DFTB molecular dynamics simulations described in section D. Calculations on selected normal modes in the 2860−2940 cm^{-1} region (see Table 2) indicate a spread of lifetimes ranging from 0.9 to 3.3 ps, spanning a similar range with that shown in Table 1. Asymmetric modes appear to be

Table 2. Calculated Vibrational Lifetimes of Selected Normal Modes

frequency[a]	mode[b]	$\langle t \rangle$/ps[c]
2862	$^{\eta\chi}CH_3$, ss	1.1 ± 0.3
2872	$^{\nu}CH_3$, ss	0.9 ± 0.7
2929	$^{\beta}CH_2$, ss	1.9 ± 0.7
2937	$^{\eta\chi}CH_3$, as	3.3 ± 0.6

[a]B3LYP/6-311++G(d,p) harmonic frequencies scaled by 0.957. [b]Abbreviations: ss = symmetric stretch, as = asymmetric stretch, χ = axial, η = endo, ν = vinylic, β = bridge position on α-pinene. [c]Averaged over five DFTB trajectories. Uncertainties correspond to 2σ (standard error) and reflect variations between runs.

longer-lived than symmetric ones presumably because of more effective transfer of vibrational energy from the latter modes. We plan to employ deuterium-labeling studies in conjunction with theoretical calculations (e.g., "on-the-fly reverse normal mode analysis")[63−65] to provide a more definitive assignment of these peaks and the pathway of IVR in future studies. In a forthcoming article, we will detail and investigate how this approach performs more broadly for the calculation of IVR rates.

We emphasize again that this level of detail in the molecular interaction and coupling can be directly revealed by the HR-BB-SFG measurement, without performing FID-SFG measurements, which are decidedly more complicated. In addition, one would assume that the time scales associated with the vibrational dephasing processes giving rise to the relatively long vibrational coherent lifetimes between 2920 and 2930 cm^{-1} are the molecular origin of the relatively large SFG signal intensities and sharp features that we generally observe from α-pinene. When the spectral resolution is not enough to capture such spectral line shape details, such detailed information on the vibrational decoherence is generally lost. This topic on the origin of the different decoherence behavior is the subject of ongoing investigations that will be reported elsewhere.

The level of accuracy in the line shapes of the HR-BB-SFG intensity spectra allows us to determine reliably, if not completely accurately, their imaginary and real parts (the so-called "phase-resolved spectra"), which may provide an alternative approach to heterodyne detection schemes[61,66−69] or analysis by the Maximum Entropy Method (MEM),[70−73] as the latter two methods also have their own limitations and inaccuracies. First, the picosecond or the femtosecond phase-resolved SFG measurements in the literature do not have high-enough spectral resolution or enough data points to resolve closely overlapping peaks as measured with the sub-1 cm^{-1} resolution measurement with the HR-BB-SFG. Second, even the MEM method can be used to retrieve the imaginary and real parts from the intensity spectra without assumption of the line shape function to obtain the spectral parameters of the overlapping peaks; a fitting of the imaginary and real parts with a certain assumption of the spectral line shape function is still needed. When the intensity spectral line shape is accurate enough, mathematically, there is little foreseeable advantage in going through the MEM process than making a direct fit of the intensity spectrum. However, one should not expect this approach of fitting the HR-BB-SFG spectra to be of additional help on systems with spectra of complicated line shape and no

apparent resolvable spectral features, such as the broad spectra of the hydrogen bond features in the 3000−3600 cm^{-1} region.[54,69]

Here, we used the spectral parameters and the simulation results that we obtained with the different spectral resolutions and calculated the imaginary and real parts of the ssp-polarized SFG spectra of α-pinene adsorbed to the CaF$_2$ surface (Figure 4). The phase-resolved spectra with 0 and 0.6 cm^{-1} spectral
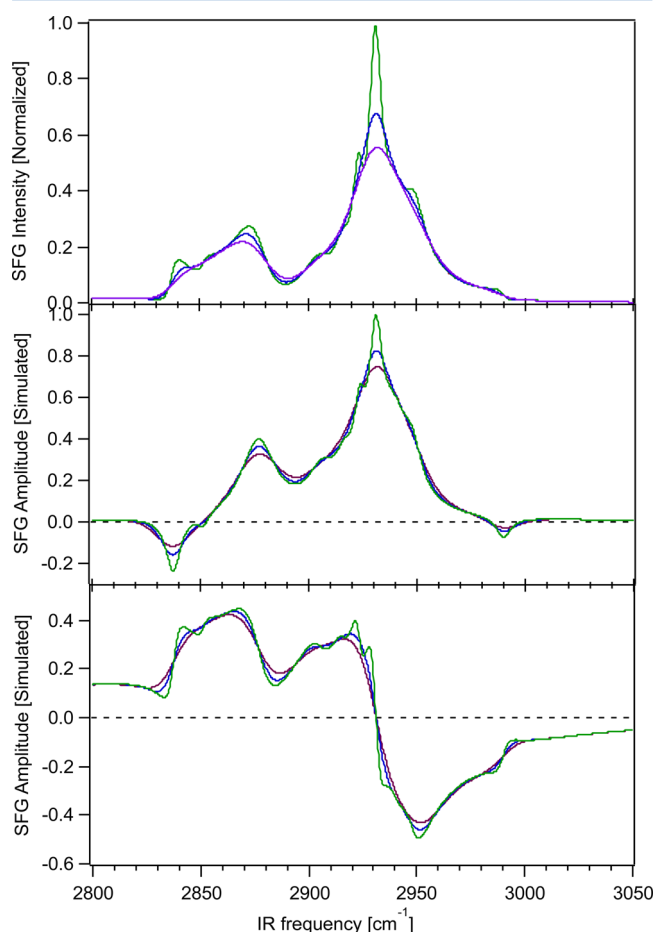
Figure 4. Comparison of the simulated intensity spectra (top), the imaginary spectra (middle), and the real spectra (bottom) of α-pinene with 0.6 (green), 6 (blue), and 10 cm^{-1} (purple) spectral resolution.

resolution overlap with each other nearly perfectly, while many details of the spectral features merge and disappear in the spectra with 6 and 15 cm^{-1} spectral resolution. We then compared the phase, that is, the sign of the amplitude parameter A_q for each peak, shown graphically in Figure 4b and listed in Table 1. In general, the phase or sign of each peak in the ssp polarization is the result of the "up" or "down" orientation of the corresponding oscillator.[63,69,74] Table 1 and Figure 4b show that two modes at the lower-frequency end and one peak at the high-frequency end are associated with opposite signs when compared to the other peaks, indicating that these three oscillators point in an opposite direction when compared to the remaining oscillators. Such phase information and the 10 resolved peaks shall allow us to make detailed spectral assignment and orientation analysis of the α-pinene molecule at the CaF$_2$ surface. As the α-pinene molecule is basically with a rigid structure, comparison between the HR-BB-SFG results and theoretical computation may help establish the benchmark

for understanding and predicting complex molecular SFG spectra, structure, and so forth. These studies are underway and shall be reported in the near future.

4. CONCLUSIONS

As established herein, we expect sub-cm^{-1} SFG spectroscopy to be of high utility for molecular spectroscopy. We have shown that HR-BB-SFG spectroscopy resolves significantly more peaks in the C−H stretching region of a highly strained hydrocarbon than conventional broad-band and scanning SFG methods. The 0.6 cm^{-1} resolution of HR-BB-SFG provides, for the first time, a nearly intrinsic line shape measurement. Time domain coherent vibrational dynamics simulations and their Fourier transformation coupled with laser profiles corresponding to different spectral resolutions reproduce the lower-resolution SFG spectra reasonably well by using the peak intensity, position, and width parameters from the spectral fits of the HR-BB-SFG spectra. Given the accurate line shapes, homogeneous vibrational decoherence lifetimes are obtained directly and without the need for time-resolved vibrational spectroscopic approaches.

At the CaF$_2$ surface, the high-resolution SFG spectrum of α-pinene is found to exhibit two vibrational modes near 2923 and 2930 cm^{-1} that exhibit vibrational decoherence lifetimes of 1.4 and 1.7 ps, respectively, which are likely to be highly sensitive to the molecular environment sampled by the oscillators. These lifetimes compare favorably to lifetimes computed from DFTB molecular dynamics calculations. Additional SFG studies of deuterium-labeled forms of α-pinene, that is, its isotopologues, are currently in progress, along with density functional theory based calculations, which will lead to reliable spectral assignments of strained hydrocarbons that exhibit strong intramolecular vibrational coupling. Additional experiments are also aimed at investigating the role of the phase (liquid versus vapor) and expand the work toward the use of different optical windows (for instance, fused silica versus CaF$_2$).

■ APPENDIX

The standard Gaussian function in the time domain is

$$g(t) = \frac{1}{\sigma\sqrt{2\pi}}e^{-t^2/2\sigma^2} \tag{1}$$

This expression satisfies the normalization condition $\int_{-\infty}^{\infty} g(t)\, dt = 1$. The fwhm of $g(t)$ is $\Delta t = 2(2\ln 2)^{1/2}\sigma \approx 2.35482\sigma$, and the Fourier transformation relationship is defined as

$$G(\omega) = \int_{-\infty}^{\infty} g(t)e^{-i\omega t}\, dt \qquad \text{and}$$

$$g(t) = \frac{1}{2\pi}\int_{-\infty}^{\infty} G(\omega)e^{i\omega t}\, d\omega \tag{2}$$

Then

$$G(\omega) = e^{-\sigma^2\omega^2/2} \tag{3}$$

and the fwhm of the frequency domain Gaussian function $G(\omega)$ is $\Delta\nu = 2(2\ln 2)^{1/2}(1/\sigma) = 2.35482(1/\sigma)$. One then arrives at

$$\Delta t \cdot \Delta\nu = 8\ln 2 \approx 5.5452$$

Now, let us consider an optical field with the Gaussian intensity distribution function

$$I(t) = |g(t)|^2 = \frac{1}{2\pi\sigma^2} e^{-t^2/\sigma^2} \tag{4}$$

Its fwhm is given by $\Delta T = (\Delta t/\sqrt{2}) = 2(\ln 2)^{1/2}\sigma$. Similarly, if in the frequency domain the Gaussian optical intensity function is

$$I(\omega) = |G(\omega)|^2 = e^{-\sigma^2\omega^2} \tag{5}$$

its fwhm is given by $\Delta\Upsilon = (\Delta\nu/\sqrt{2}) = (2\ln 2)^{1/2}(1/\sigma)$. Therefore, one arrives at

$$\Delta T \cdot \Delta\Upsilon = 4\ln 2 \approx 2.7726 \tag{6}$$

If ΔT has units of ps and $\Delta\Upsilon$ has units of cm^{-1}, one obtains

$$\Delta T \cdot \Delta\Upsilon = \frac{4\ln 2 \times 10^{12}}{2 \times \pi \times 3 \times 10^{10}} \approx 14.709. \tag{7}$$

Therefore, if $\Delta T = 2.5$ ps, then $\Delta\Upsilon = 5.88$ cm^{-1}, and if $\Delta T = 1.5$ ps, then $\Delta\Upsilon = 9.81$ cm^{-1}.

Similarly, one obtains $\Delta t \cdot \Delta\nu = (2^{1/2}\Delta T) \cdot (2^{1/2}\Delta\Upsilon) = 2\Delta T \cdot \Delta\Upsilon \approx 29.418$.

Spectral resolution in SFG spectroscopy is the fwhm of the spectral intensity of the visible pulse, that is, $\Delta\Upsilon$ of the visible pulse spectrum, while the time resolution of the visible upconverter pulse is the fwhm of the time-domain intensity of the visible pulse, that is, ΔT of the visible pulse temporal profile. Therefore, one should use the relationship $\Delta T \cdot \Delta\Upsilon \approx 14.709$ in estimating the spectral resolution and time width of the upconverter pulse in SFG spectroscopy.

ASSOCIATED CONTENT

ⓈSupporting Information

Synthesis of $(-)$-α-pinene, (1R)-6,6-dimethylbicyclo[3.1.1]-heptan-2-one, (1R)-6,6-dimethylbicyclo[3.1.1]hept-2-en-2-yl trifluoromethanesulfonate, and (1S)-6,6-dimethy-2-bicyclo-[3.1.1]hept-2-ene, ssp-polarized high-resolution SFG spectra, simulated time domain SFG free-induction decay curve, DFTB calculations, dependence of computed vibrational lifetimes on step size, and decay of displacement along the normal mode and corresponding Lorentzian fit to the Fourier transform. This material is available free of charge via the Internet at http://pubs.acs.org.

AUTHOR INFORMATION

Corresponding Authors
*E-mail: hongfei.wang@pnnl.gov (H.-F.W.).
*E-mail: geigerf@chem.northwestern.edu (F.M.G..).

Present Addresses
▽L.V.: Chemistry Department, University at Buffalo, Buffalo, NY 14260.
#C.J.E.: Chemistry Department, University of California, Berkeley, CA 94720.
¶Z.L.: Beijing National Laboratory for Molecular Sciences, Institute of Chemistry, the Chinese Academy of Sciences, Beijing 100190, China.

Author Contributions
⊥A.L.M. and L.V. contributed equally to this work.

Notes
The authors declare no competing financial interest.

ACKNOWLEDGMENTS

REFERENCES

(1) Phillips, M. A.; Wildung, M. R.; Williams, D. C.; Hyatt, D. C.; Croteau, R. CdNa Isolation, Functional Expression, and Characterization of (+)-α-Pinene Synthase and ($-$)-α-Pinene Synthase from Loblolly Pine (Pinus Taeda): Stereocontrol in Pinene Biosynthesis. *Arch. Biochem. Biophys.* 2003, 411, 267−276.

(2) Stephanou, E. G. A Forest Air of Chirality, Nature News and Views. *Nature* 2007, 446, 991.

(3) Trnka, T. M.; Grubbs, R. H. The Development of L₂X₂Ru=CHR Olefin Metathesis Catalysts: An Organometallic Success Story. *Acc. Chem. Res.* 2001, 34, 18−29.

(4) Wilson, H. W. The Infrared and Raman Spectra of α- and β-Pinenes. *Appl. Spectrosc.* 1976, 30, 209−212.

(5) Calogirou, A.; Larsen, B. R.; Kotzias, D. Gas-Phase Terpene Oxidation Products: A Review. *Atmos. Environ.* 1999, 33, 1423−1439.

(6) Abbate, S.; Longhi, G.; Ricard, L.; Bertucci, C.; Rosini, C.; Salvadori, P.; Moscowitz, A. Vibrational Circular Dichroism as a Criterion for Local-Mode versus Normal-Mode Behavior. Near-Infrared Circular Dichroism Spectra of Some Monoterpenes. *J. Am. Chem. Soc.* 1989, 111, 836−840.

(7) Cheeseman, J. R.; Frisch, M. J. Basis Set Dependence of Vibrational Raman and Raman Optical Activity Intensities. *J. Chem. Theory Comput.* 2011, 7, 3323−3334.

(8) Shen, Y. R. Surface-Properties Probed by 2nd-Harmonic and Sum-Frequency Generation. *Nature* 1989, 337, 519−525.

(9) Eisenthal, K. B. Liquid Interfaces Probed by Second-Harmonic and Sum-Frequency Spectroscopy. *Chem. Rev.* 1996, 96, 1343−1360.

(10) Wang, H. F.; Gan, W.; Lu, R.; Rao, Y.; Wu, B. H. Quantitative Spectral and Orientational Analysis in Surface Sum Frequency Generation Vibrational Spectroscopy (SFG-VS). *Int. Rev. Phys. Chem.* 2005, 24, 191−256.

(11) Geiger, F. M. Second Harmonic Generation, Sum Frequency Generation, and χ^3: Dissecting Environmental Interfaces with a Nonlinear Optical Swiss Army Knife. *Annu. Rev. Phys. Chem.* 2009, 60, 61−83.

(12) Richmond, G. L. Structure and Bonding of Molecules at Aqueous Surfaces. *Annu. Rev. Phys. Chem.* 2001, 52, 357−389.

(13) Lu, R.; Gan, W.; Wu, B. H.; Zhang, Z.; Guo, Y.; Wang, H. F. C−H Stretching Vibrations of Methyl, Methylene and Methine Groups at the Vapor/Alcohol ($N = 1−8$) Interfaces. *J. Phys. Chem. B* 2005, 109, 14118−14129.

(14) Lu, R.; Gan, W.; Wu, B. H.; Chen, H.; Wang, H. F. Vibrational Polarization Spectroscopy of Ch Stretching Modes of the Methylene Goup at the Vapor/Liquid Interfaces with Sum Frequency Generation. *J. Phys. Chem. B* 2004, 108, 7297−7306.

(15) Velarde, L.; Wang, H. F. Unified Treatment and Measurement of the Spectral Resolution and Temporal Effects in Frequency-Resolved Sum-Frequency Generation Vibrational Spectroscopy (SFG-VS). *Phys. Chem. Chem. Phys.* **2013**, *15*, 19970−19984.

(16) Gan, W.; Wu, B. H.; Zhang, Z.; Guo, Y.; Wang, H. F. Vibrational Spectra and Molecular Orientation with Experimental Configuration Analysis in Surface Sum Frequency Generation (SFG). *J. Phys. Chem. C* **2007**, *111*, 8716−8725.

(17) Gan, W.; Zhang, Z.; Feng, R. R.; Wang, H. F. Spectral Interference and Molecular Conformation at Liquid Interface with Sum Frequency Generation Vibrational Spectroscopy (SFG-VS). *J. Phys. Chem. C* **2007**, *111*, 8726−8738.

(18) Velarde, L.; Zhang, X.-y.; Lu, Z.; Joly, A. G.; Wang, Z.; Wang, H.-f. Spectroscopic Phase and Lineshapes in High-Resolution Broadband Sum Frequency Vibrational Spectroscopy: Resolving Interfacial Inhomogeneities of "Identical" Molecular Groups. *J. Chem. Phys.* **2011**, *135*, 241102.

(19) Rivera, C. A.; Fourkas, J. T. Reexamining the Interpretation of Vibrational Sum-Frequency Generation Spectra. *Int. Rev. Phys. Chem.* **2011**, *30*, 409−443.

(20) Buchbinder, A. M.; Gibbs-Davis, J. M.; Stokes, G. Y.; Peterson, M. D.; Weitz, E.; Geiger, F. M. Method for Evaluating Vibrational Mode Assignments in Surface-Bound Cyclic Hydrocarbons Using Sum-Frequency Generation. *J. Phys. Chem. C* **2011**, *115*, 18284−18294.

(21) Ebben, C. J.; et al. Contrasting Organic Aerosol Particles from Boreal and Tropical Forests During Humppa-Copec-2010 and Amaze-08 Using Coherent Vibrational Spectroscopy. *Atmos. Chem. Phys.* **2011**, *11*, 10317−10329.

(22) Lu, Z.; Karakoti, A.; Velarde, L.; Wang, W.; Yang, P.; Thevuthasan, S.; Wang, H.-f. Dissociative Binding of Carboxylic Acid Ligand on Nanoceria Surface in Aqueous Solution: A Joint in Situ Spectroscopic Characterization and First-Principles Study. *J. Phys. Chem. C* **2013**, 24329−24338.

(23) Esenturk, O.; Walker, R. A. Surface Structure at Hexadecane and Halo-Hexadecane Liquid/Vapor Interfaces. *J. Phys. Chem. B* **2004**, *108*, 10631−10635.

(24) Voges, A. B.; Al-Abadeh, H. A.; Musorrafiti, M. J.; Bertin, P. A.; Nguyen, S. T.; Geiger, F. M. Carboxylic Acid- and Ester-Functionalized Siloxane Scaffolds on Glass Studied by Broadband Sum Frequency Generation. *J. Phys. Chem. B* **2004**, *108*, 18675−18682.

(25) McCamant, D. W.; Kukura, P.; Mathies, R. A. Femtosecond Broadband Stimulated Raman: A New Approach for High-Performance Vibrational Spectroscopy. *Appl. Spectrosc.* **2003**, *57*, 1317−1323.

(26) Umapathy, S.; Lakshmanna, A.; Mallick, B. Ultrafast Raman Loss Spectroscopy. *J. Raman Spectrosc.* **2009**, *40*, 235−237.

(27) Aradi, B.; Hourahine, B.; Frauenheim, T. DFTB+, a Sparse Matrix-Based Implementation of the DFTB Method. *J. Phys. Chem. A* **2007**, *111*, 5678.

(28) Elstner, M.; Porezag, D.; Jungnickel, G.; Elsner, M.; Haugk, M.; Frauenheim, T.; Suhai, S.; Seifert, G. *Phys. Rev. B* **1998**, *58*, 7260.

(29) Pleiss, J.; Jahnig, F. *Biophys. J.* **1991**, *59*, 795−804.

(30) Beu, T. A.; Onoe, J.; Takeuchi, K. *Eur. Phys. J. D* **2001**, *17*, 205−212.

(31) Baer, M.; Mathias, G.; Kuo, I.-F.; Tobias, D. J.; Mundy, C. J.; Marx, D. *ChemPhysChem* **2008**, *9*, 2703−2707.

(32) Stare, J.; Mavri, J.; Grdadolnik, J.; Zidar, J.; Maksic, Z. B.; Vianello, R. Hydrogen Bond Dynamics of Histamine Monocation in Aqueous Solution: Car−Parrinello Molecular Dynamics and Vibrational Spectroscopy Study. *J. Phys. Chem. B* **2011**, *115*, 5999−6010.

(33) Buchbinder, A. M.; Weitz, E.; Geiger, F. M. Pentane, Hexane, Cyclopentane, Cyclohexane, 1-Hexene, 1-Pentene, *cis*-2-Pentene, Cyclohexene, and Cyclopentene at Vapor/α-Alumina and Liquid/α-Alumina Interfaces Studied by Broadband Sum Frequency Generation. *J. Phys. Chem. C* **2010**, *114*, 554−566.

(34) Bellamy, L. J. *The Infra-Red Spectra of Complex Molecules*; John Wiley & Sons: New York, 1975; p 433.

(35) Roeges, N. P. G. *A Guide to the Complete Interpretation of Infrared Spectra of Organic Structures*; John Wiley & Sons: New York, 1994.

(36) Guyot-Sionnest, P.; Hunt, J. H.; Shen, Y. R. Sum-Frequency Vibrational Spectroscopy of a Langmuir Film: Study of Molecular Orientation of a Two-Dimensional System. *Phys. Rev. Lett.* **1987**, *59*, 1597−1600.

(37) Dollish, F. R.; Fateley, W. G.; Bentley, F. F. *Characteristic Raman Frequencies of Organic Compounds*; John Wiley & Sons: New York, 1974; p 443.

(38) Esenturk, O.; Walker, R. A. Surface Vibrational Structure at Alkane Liquid/Vapor Interfaces. *J. Chem. Phys.* **2006**, *125*, 174701.

(39) Voges, A. B.; Stokes, G. Y.; Gibbs-Davis, J. M.; Lettan, R. B.; Bertin, P. A.; Pike, R. C.; Nguyen, S. T.; Scheidt, K. A.; Geiger, F. M. Insights into Heterogeneous Atmospheric Oxidation Chemistry: Development of a Tailor-Made Synthetic Model for Studying Tropospheric Surface Chemistry. *J. Phys. Chem. C* **2007**, *111*, 1567−1578.

(40) Sefler, G. A.; Du, Q.; Miranda, P. B.; Shen, Y. R. Surface Crystallization of Liquid N-Alkanes and Alcohol Monolayers Studied by Surface Vibrational Spectroscopy. *Chem. Phys. Lett.* **1995**, *235*, 347−354.

(41) Nanjundiah, K.; Dhinojwala, A. Confinement-Induced Ordering of Alkanes between an Elastomer and a Solid Surface. *Phys. Rev. Lett.* **2005**, *95*, 154301.

(42) Chen, C. Y.; Even, M. A.; Wang, J.; Chen, Z. Sum Frequency Generation Vibrational Spectroscopy Studies on Molecular Conformation of Liquid Polymers Poly(ethylene glycol) and Poly-(propylene glycol) at Different Interfaces. *Macromolecules* **2002**, *35*, 9130−9135.

(43) Opdahl, A.; Phillips, R. A.; Somorjai, G. A. Surface Segregation of Methyl Side Branches Monitored by Sum Frequency Generation (SFG) Vibrational Spectroscopy for a Series of Random Poly-(ethylene-*co*-propylene) Copolymers. *J. Phys. Chem. B* **2002**, *106*, 5212−5220.

(44) Miranda, P. B.; Shen, Y. R. Liquid Interfaces: A Study by Sum-Frequency Vibrational Spectroscopy. *J. Phys. Chem. B* **1999**, *103*, 3292−3307.

(45) Conboy, J. C.; Messmer, M. C.; Richmond, G. L. Dependence of Alkyl Chain Conformation of Simple Ionic Surfactants on Head Group Functionality as Studied by Vibrational Sum-Frequency Spectroscopy. *J. Phys. Chem. B* **1997**, *101*, 6724−6733.

(46) Conboy, J. C.; Messmer, M. C.; Richmond, G. L. Effect of Alkyl Chain Length on the Conformation and Order of Simple Ionic Surfactants Adsorbed at the D_2O/CCl_4 Interface as Studied by Sum-Frequency Vibrational Spectroscopy. *Langmuir* **1998**, *14*, 6722−6727.

(47) Wang, C.-Y.; Groenzin, H.; Schultz, M. J. Molecular Species on Nanoparticulate Anatase TiO_2 Film Detected by Sum Frequency Generation: Trace Hydrocarbons and Hydroxyl Groups. *Langmuir* **2003**, *19*, 7330−7334.

(48) Wang, C. Y.; Groenzin, H.; Shultz, M. J. Surface Characterization of Nanoscale TiO_2 Film by Sum Frequency Generation Using Methanol as a Molecular Probe. *J. Phys. Chem. B* **2004**, *108*, 265−272.

(49) Voges, A. B.; Al-Abadleh, H. A.; Geiger, F. M. Applications of Nonlinear Optical Techniques for Studying Heterogeneous Systems Relevant in the Natural Environment. In *Environmental Catalysis*; Grassian, V. H., Ed.; CRC Press: Boca Raton, FL, 2005; pp 83−128.

(50) Ball, D. W. Density Functional Calculations on the Heats of Formation of Cyclic Hydrocarbons. *J. Mol. Struct.: THEOCHEM* **1997**, *417*, 107−115.

(51) Durig, J. R.; El Defrawy, A. M.; Ward, R. M.; Guirgis, G. A.; Gounev, T. K. Conformational Stability of Chlorocyclohexane from Temperature-Dependent FT-IR Spectra of Xenon Solutions, R(0) Structural Parameters, and Vibrational Assignment. *Struct. Chem.* **2008**, *19*, 579−594.

(52) Durig, J. R.; Lee, M. J.; Little, T. S. Spectra and Structure of Small Ring Compounds. Part LVI- Raman and Far-Infrared Spectra, Conformational Stability Vibrational Assignments, Normal Coordinate

Analysis and *Ab Initio* Calculations of Chlorocyclobutane. *J. Raman Spectrosc.* **1990**, *21*, 529−542.

(53) Galabov, B.; Simov, D. Stretching Vibrations of Methylene Group and Ring Strain in Cycloalkanes. *J. Mol. Struct.* **1972**, *11*, 341.

(54) Wang, H.-F.; Velarde, L.; Gan, W.; Fu, L. Quantitative Sum-Frequency Generation Vibrational Spectroscopy of Molecular Surfaces and Interfaces: Lineshape, Polarization, and Orientation. *Annu. Rev. Phys. Chem.* **2015**, *66*, 189−216.

(55) Chen, H.; Gan, W.; Wu, B.-h.; Wu, D.; Zhang, Z.; Wang, H.-f. Determination of the Two Methyl Group Orientations at Vapor/Acetone Interface with Polarization Null Angle Method in SFG Vibrational Spectroscopy. *Chem. Phys. Lett.* **2005**, *408*, 284−289.

(56) Achtyl, J. L.; Buchbinder, A. M.; Geiger, F. M. Hydrocarbon on Carbon: Coherent Vibrational Spectroscopy of Toluene on Graphite. *J. Phys. Chem. Lett.* **2012**, *3*, 280−282.

(57) Ebben, C. J.; Strick, B. F.; Upshur, M. A.; Chase, H. M.; Achtyl, J. L.; Thomson, R. J.; Geiger, F. M. Towards the Identification of Molecular Constituents Associated with the Surfaces of Isoprene-Derived Secondary Organic Aerosol (SOA) Particles. *Atmos. Chem. Phys.* **2014**, *14*, 2303−2314.

(58) Long, D. A. *The Raman Effect: A Unified Treatment of the Theory of Raman Scattering by Molecules*; Wiley: New York, 2002.

(59) Carter, J. A.; Wang, Z. H.; Dlott, D. D. Ultrafast Nonlinear Coherent Vibrational Sum-Frequency Spectroscopy Methods to Study Thermal Conductance of Molecules at Interfaces. *Acc. Chem. Res.* **2009**, *42*, 1343−1351.

(60) Weeraman, C.; Mitchell, S. A.; Lausten, R.; Johnston, L. J.; Stolow, A. Vibrational Sum Frequency Generation Spectroscopy Using Inverted Visible Pulses. *Opt. Express* **2010**, *18*, 11483−11494.

(61) Shalhout, F. Y.; Malyk, S.; Benderskii, A. V. Relative Phase Change of Nearby Resonances in Temporally Delayed Sum Frequency Spectra. *J. Phys. Chem. Lett.* **2012**, *3*, 3493−3497.

(62) Velarde, L.; Wang, H. F. Capturing Inhomogeneous Broadening of the −CN Stretch Vibration in a Langmuir Monolayer with High-Resolution Spectra and Ultrafast Vibrational Dynamics in Sum-Frequency Generation Vibrational Spectroscopy (SFG-VS). *J. Chem. Phys.* **2013**, *139*, 084204.

(63) Czako, G.; Bowman, J. M. *J. Chem. Phys.* **2009**, *131*, 244302.

(64) Czako, G.; Kaledin, A. L.; Bowman, J. M. *J. Chem. Phys.* **2010**, *132*, 164103.

(65) Takahashi, K. *Phys. Chem. Chem. Phys.* **2010**, *12*, 13950−13961.

(66) Stiopkin, I. V.; Jayathilake, H.; Bordenyuk, A. N.; Benderskii, A. V. Heterodyne-Detected Vibrational Sum Frequency Generation Spectroscopy. *J. Am. Chem. Soc.* **2008**, *130*, 2271−2275.

(67) Covert, P. A.; FitzGerald; Hore, D. K. Simultaneous Measurement of Magnitude and Phase in Interferometric Sum-Frequency Vibrational Spectroscopy. *J. Chem. Phys.* **2012**, *137*, 014201.

(68) Mondal, J. A.; Nihonyanagi, S.; Yamaguchi, S.; Tahara, T. Structure and Orientation of Water at Charged Lipid Monolayer/Water Interfaces Probed by Heterodyne-Detected Vibrational Sum Frequency Generation Spectroscopy. *J. Am. Chem. Soc.* **2010**, *132*, 10656−10657.

(69) Shen, Y. R. Phase-Sensitive Sum-Frequency Spectroscopy. *Annu. Rev. Phys. Chem.* **2013**, *64*, 129−150.

(70) de Beer, A. G. F.; Samson, J. S.; Hua, W.; Huang, Z. S.; Chen, X. K.; Allen, H. C.; Roke, S. Direct Comparison of Phase-Sensitive Vibrational Sum Frequency Generation with Maximum Entropy Method: Case Study of Water. *J. Chem. Phys.* **2011**, *135*, 224701.

(71) de Beer, A. G. F.; Chen, Y.; Scheu, R.; Conboy, J. C.; Roke, S. Analysis of Complex Spectra Using Fourier Filtering. *J. Phys. Chem. C* **2013**, *117*, 26582−26587.

(72) Yang, P. K.; Huang, J. Y. Phase-Retrieval Problems in Infrared-Visible Sum-Frequency Generation Spectroscopy by the Maximum-Entropy Method. *J. Opt. Soc. Am. B: Opt. Phys.* **1997**, *14*, 2443−2448.

(73) Sovago, M.; Vartiainen, E.; Bonn, M. Determining Absolute Molecular Orientation at Interfaces: A Phase Retrieval Approach for Sum Frequency Generation Spectroscopy. *J. Phys. Chem. C* **2009**, *113*, 6100−6106.

(74) Velarde, L.; Wang, H. F. Unique Determination of the −CN Group Tilt Angle in Langmuir Monolayers Using Sum-Frequency Polarization Null Angle and Phase. *Chem. Phys. Lett.* **2013**, *585*, 42−48.